








Publication Year	2017
Acceptance in OA @INAF	2021-01-07T15:36:09Z
Title	AGILE Observations of the Gravitational-wave Source GW170104
Authors	VERRECCHIA, Francesco; TAVANI, MARCO; URSI, ALESSANDRO; ARGAN, ANDREA; PITTORI, Carlotta; et al.
DOI	10.3847/2041-8213/aa8224
Handle	http://hdl.handle.net/20.500.12386/29568
Journal	THE ASTROPHYSICAL JOURNAL LETTERS
Number	847



AGILE Observations of the Gravitational-wave Source GW170104

F. Verrecchia^{1,2}, M. Tavani^{3,4,5} , A. Ursi³, A. Argan³, C. Pittori^{1,2}, I. Donnarumma⁶, A. Bulgarelli⁷, F. Fuschino⁷, C. Labanti⁷, M. Marisaldi⁸, Y. Evangelista³, G. Minervini³, A. Giuliani⁹, M. Cardillo³, F. Longo¹⁰, F. Lucarelli^{1,2}, P. Munar-Adrover¹¹ , G. Piano³ , M. Pilia¹², V. Fioretti⁷, N. Parmiggiani⁷, A. Trois¹², E. Del Monte³, L. A. Antonelli^{1,2}, G. Barbiellini¹⁰, P. Caraveo⁹, P. W. Cattaneo¹³, S. Colafrancesco¹⁴, E. Costa^{3,6}, F. D’Amico⁶, M. Feroci³, A. Ferrari¹⁵, A. Morselli¹⁶ , L. Pacciani³, F. Paoletti^{3,17}, A. Pellizzoni¹², P. Picozza¹⁶, A. Rappoldi¹³, and S. Vercellone¹⁸ 

¹ASI Space Science Data Center (SSDC), via del Politecnico, I-00133 Roma, Italy

²INAF-OAR, via Frascati 33, I-00078 Monte Porzio Catone (Roma), Italy

³INAF-IAPS, via del Fosso del Cavaliere 100, I-00133 Roma, Italy

⁴Dipartimento di Fisica, Università di Roma “Tor Vergata,” via della Ricerca Scientifica 1, I-00133 Roma, Italy

⁵Gran Sasso Science Institute, viale Francesco Crispi 7, I-67100 L’Aquila, Italy

⁶ASI, via del Politecnico snc, I-00133 Roma, Italy

⁷INAF-IASF-Bologna, via Gobetti 101, I-40129 Bologna, Italy

⁸Birkeland Centre for Space Science, Department of Physics and Technology, University of Bergen, Bergen, Norway

⁹INAF-IASF Milano, via E. Bassini 15, I-20133 Milano, Italy

¹⁰Dipartimento di Fisica, Università di Trieste and INFN, via Valerio 2, I-34127 Trieste, Italy

¹¹Unitat de Física de les Radiacions, Departament de Física, and CERES-IEEC, Universitat Autònoma de Barcelona, E-08193 Bellaterra, Spain

¹²INAF, Osservatorio Astronomico di Cagliari, via della Scienza 5, I-09047 Selargius (CA), Italy

¹³INFN-Pavia, via Bassi 6, I-27100 Pavia, Italy

¹⁴University of Witwatersrand, Johannesburg, South Africa

¹⁵CIFS, c/o Physics Department, University of Turin, via P. Giuria 1, I-10125 Torino, Italy

¹⁶INFN Roma Tor Vergata, via della Ricerca Scientifica 1, I-00133 Roma, Italy

¹⁷East Windsor RSD, 25A Leshin Lane, Hightstown, NJ 08520, USA

¹⁸INAF, Osservatorio Astronomico di Brera, via Emilio Bianchi 46, I-23807 Merate (LC), Italy

Received 2017 May 31; revised 2017 July 19; accepted 2017 July 20; published 2017 September 28

Abstract

The LIGO/Virgo Collaboration (LVC) detected on 2017 January 4 a significant gravitational-wave (GW) event (now named GW170104). We report in this Letter the main results obtained from the analysis of hard X-ray and gamma-ray data of the AGILE mission that repeatedly observed the GW170104 localization region (LR). At the LVC detection time T_0 AGILE observed about 36% of the LR. The gamma-ray imaging detector did not reveal any significant emission in the energy range 50 MeV–30 GeV. Furthermore, no significant gamma-ray transients were detected in the LR that was repeatedly exposed over timescales of minutes, hours, and days. We also searched for transient emission using data near T_0 of the omnidirectional detector MCAL operating in the energy band 0.4–100 MeV. A refined analysis of MCAL data shows the existence of a weak event (that we call “E2”) with a signal-to-noise ratio of 4.4σ lasting about 32 ms and occurring 0.46 ± 0.05 s before T_0 . A study of the MCAL background and of the false-alarm rate of E2 leads to the determination of a post-trial significance between 2.4σ and 2.7σ for a temporal coincidence with GW170104. We note that E2 has characteristics similar to those detected from the weak precursor of GRB 090510. The candidate event E2 is worth consideration for simultaneous detection by other satellites. If associated with GW170104, it shows emission in the MeV band of a short burst preceding the final coalescence by 0.46 s and involving $\sim 10^{-7}$ of the total rest mass energy of the system.

Key words: gamma rays; general – gravitational waves

1. Introduction

The LIGO/Virgo Collaboration (LVC) detected a gravitational-wave (GW) event on 2017 January 4 (The LIGO Scientific Collaboration & Virgo Collaboration 2017a, 2017b, 2017c). This event, originally labeled G268556, occurred at time $T_0 = 10:11:58.599$ UTC; it is now named GW170104 (Abbott et al. 2017, hereafter A17). The event is identified as a compact binary coalescence (CBC) of two black holes of masses $\sim 31 M_\odot$ and $\sim 19 M_\odot$. The estimated distance is 880_{-390}^{+450} Mpc corresponding to a redshift of $z = 0.18_{-0.07}^{+0.08}$. GW170104 is an event of great interest because its “false-alarm rate” (FAR) is less than 1 in 70,000 years as determined by a refined analysis (A17). This event is the third of a set of high-significance and confirmed GW events detected by LVC, the first one being GW150914 and the second one being GW151226 (Abbott et al. 2016a, 2016b, 2016c, 2016d, 2016e, 2016f).

A first sky map of GW170104 was distributed through a LVC-GCN on 2017 January 4 (The LIGO Scientific Collaboration & Virgo Collaboration 2017a), including an initial localization generated by the BAYESTAR pipeline (Singer & Price 2016). An updated sky map was distributed on 2017 January 17 (The LIGO Scientific Collaboration & Virgo Collaboration 2017c), based on LALInference (Veitch et al. 2015). The probability is concentrated in two long, thin arcs in the sky. The 50% credible region spans about 500 deg^2 and the 90% region about 2000 deg^2 . A final sky map was issued on 2017 May 17 (The LIGO Scientific Collaboration & Virgo Collaboration 2017b). AGILE reacted to the initial LVC notification of GW170104 and started a quicklook analysis within a few hours as discussed below (Tavani et al. 2017a, 2017b). In the following, we name the two arcs of the GW170104 LR differently: the northern arc is named “A,” and the southern arc is named “B.”

In this Letter, we present the main results of the analysis of AGILE data concerning GW170104. Section 2 summarizes the observation capability of AGILE for the search of GW event counterparts. Section 3 presents the results concerning gamma-ray emission above 50 MeV from GW170104. Section 4 includes the analysis of gamma-ray data obtained by the MCAL detector in the energy range 0.4–100 MeV with a discussion of an interesting candidate event occurring near T_0 . Section 5 presents a brief discussion of our results, and conclusions are reported in Section 6.

2. The AGILE Satellite Searching for GW Event Counterparts

The AGILE satellite that is orbiting the Earth in a near equatorial orbit at an altitude of ~ 500 km (Tavani et al. 2009) is currently exposing 80% of the entire sky every 7 minutes in a “spinning mode.” The instrument consists of an imaging gamma-ray Silicon Tracker (sensitive in the energy range 30 MeV–30 GeV), Super-AGILE (SA; operating in the energy range 20–60 keV), and the Mini-Calorimeter (MCAL; working in the range 0.35–100 MeV; Labanti et al. 2009; Marisaldi et al. 2008; Fuschino et al. 2008) with an omnidirectional field of view (FoV) and self-triggering capability in burst mode for various trigger timescales. The anticoincidence (AC) system completes the instrument (for a summary of the AGILE mission features, see Tavani et al. 2009). The combination of Tracker, MCAL, and AC working as a gamma-ray imager constitutes the AGILE-GRID. The instrument is capable of detecting gamma-ray transients and GRB-like phenomena on timescales ranging from submilliseconds to tens of hundreds of seconds. In preparation of the Advanced LIGO second Observing run (O2) and the first Advanced Virgo one, the AGILE data acquisition system and trigger configuration were substantially improved. The data obtained for GW170104 greatly benefited from this improvement.

Both MCAL and SA are particularly efficient in detecting GRBs of the long and short classes as demonstrated in recent years¹⁹. Because of its triggering capabilities, in particular a special submillisecond search for transient events detected by MCAL (Labanti et al. 2009; Tavani et al. 2009), AGILE so far has further detected more than 1000 terrestrial gamma-ray flashes with durations ranging from hundreds to thousands of microseconds (Marisaldi et al. 2014; Tavani et al. 2011).

The characteristics that make AGILE in spinning mode an important instrument for follow-up observations of wide GW source LRs are: a very large FoV of the GRID (2.5 sr), an accessible region of 80% of the whole sky that can be exposed every 7 minutes, 100–150 useful passes every day for any region in the accessible sky, a gamma-ray exposure of ~ 2 minutes of any field in the accessible sky every 7 minutes, sensitivity of $\sim 10^{-8}$ erg cm $^{-2}$ s $^{-1}$ above 30 MeV for typical single-pass of unocculted sky regions, a submillisecond MCAL trigger for very fast events in the range 0.4–100 MeV, and hard X-ray (20–60 keV) triggers of GRB-like events with a localization accuracy of 2–3 arcmin in the SA FoV (~ 1 sr) when operating in imaging mode.

¹⁹ GRB 080514B (Giuliani et al. 2008), GRB 090401B (Moretti et al. 2009), GRB 090510 (Giuliani et al. 2010), GRB 100724B (Del Monte et al. 2011), an evaluation of GRID upper limits for a sample of GRB in Longo et al. (2012), GRB 130327B (Longo et al. 2013), GRB 130427A (Verrecchia et al. 2013), GRB 131108A (Giuliani et al. 2013, 2014), and the first catalog of GRBs detected by MCAL (Galli et al. 2013).

Satellite data are transmitted to the ground currently on average every passage over the ASI Malindi ground station in Kenya. Scientific data are then processed by a fast processing that was recently improved for the search of electromagnetic (e.m.) counterparts of GW sources. The current data processing can typically produce an alert for a transient gamma-ray source and/or GRB-like events within 20 minutes–2 hr from satellite onboard acquisition (Bulgarelli et al. 2014; Pittori 2013).

3. GRID Observations of GW170104

3.1. Prompt Emission

AGILE sky scanning observation covered the GW170104 event (at time $T_0 = 10:11:58.599$ UTC on 2017 January 4; The LIGO Scientific Collaboration & Virgo Collaboration 2017a) with the GRID FoV only marginally occulted by the Earth. Figure 1 shows the gamma-ray sensitivity map above 50 MeV at the GW170104 detection time. The Earth partially covers the lower part of the B arc (obtained from the 90% GW170104 LR from the refined localization map; A17). The remaining part of the B arc and a small area of the upper A arc (A2) are not occulted and inside the AGILE exposure region. We performed a search for (1) the prompt event involving the GRID, MCAL, AC, and SA and (2) precursor and delayed emission on multiple timescales involving the GRID. Interestingly, the AGILE-GRID exposed a good fraction (36%) of the B arc on time interval of about 200 s centered at T_0 .

No significant gamma-ray emission was detected by the GRID near T_0 . We obtained 3σ flux upper limits (ULs) in the band 50 MeV–10 GeV, $UL = 1.8 \times 10^{-6}$ erg cm $^{-2}$ s $^{-1}$ and $UL = 2.9 \times 10^{-8}$ erg cm $^{-2}$ s $^{-1}$ for 2 s and 100 s integrations, respectively. As shown in Figure 2, we compare our gamma-ray ULs for GW170104 with the short GRB 090510 gamma-ray light curve detected by AGILE (Giuliani et al. 2010). The short GRB 090510 (at the redshift $z = 0.9$) has been considered a reference for potential electromagnetic gamma-ray emission that could be associated to a GW event (Ackermann et al. 2016; Tavani et al. 2016). In Figure 2, we show the GRB 090510 light curve rescaled (in flux and time corrected) as if it were emitted at the GW170104 estimated distance ($z = 0.18$).

3.2. Precursor and Delayed Emission

AGILE was also optimally positioned in the GW170104 LR at interesting time intervals preceding and following the prompt event. We show in Figure 3 the sequence of passes of 100 s duration over the LR within $T_0 \pm 1000$ s, and we summarize in Table 1 the 3σ flux UL range, minimum and maximum value within the covered LR portion. We label time intervals of the highest GRID exposure with progressive numbers with respect to the prompt interval Δ_0 . It is interesting to note that exposures obtained from Table 1 reached 60%–70% of the LR. We also carried out a long-timescale search for transient gamma-ray emission during the hours immediately following or anticipating the prompt event. No significant gamma-ray emission in the GW170104 LR was detected over timescales of hours up to two-day integrations.

4. Analysis of MCAL Data and Identification of an Interesting Event

The onboard MCAL processing procedure identified an above-threshold event that triggered full telemetry data

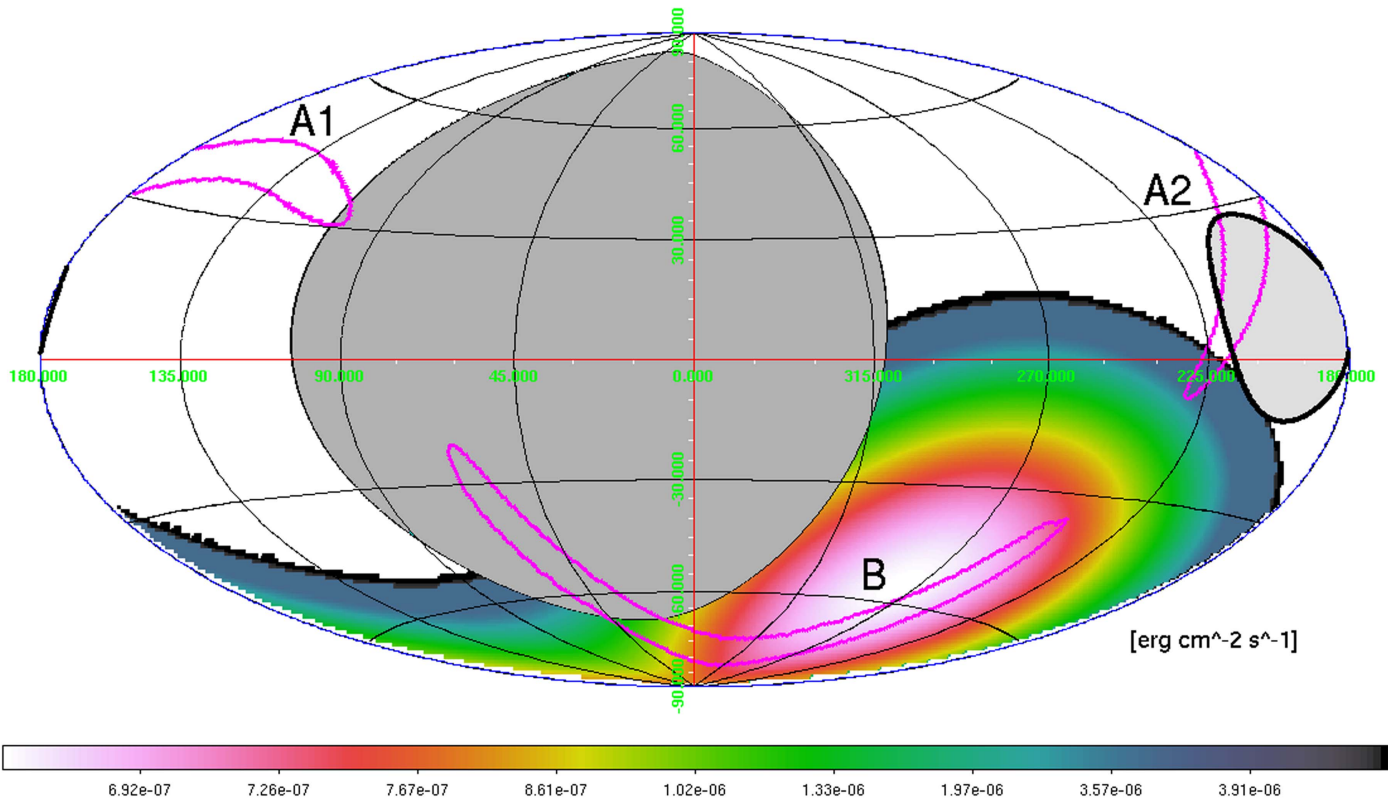


Figure 1. AGILE-GRID $E > 50$ MeV sensitivity map (in $\text{erg cm}^{-2} \text{s}^{-1}$) in Galactic coordinates based on the gamma-ray exposure at the detection time T_0 of GW170104. The shadowed areas show the Earth-occulted region and the sky fraction not directly accessible by AGILE for solar panel constraints. The magenta contours show the LALInference 90% c.l. LR of GW170104 (The LIGO Scientific Collaboration & Virgo Collaboration 2017c). The two parts of the northern arc of the LR are marked with “A1” and “A2” while the southern arc is marked by “B.” The AGILE instrument has significant exposure of the B-region at T_0 , covering about 35% of the total LR of GW170104.

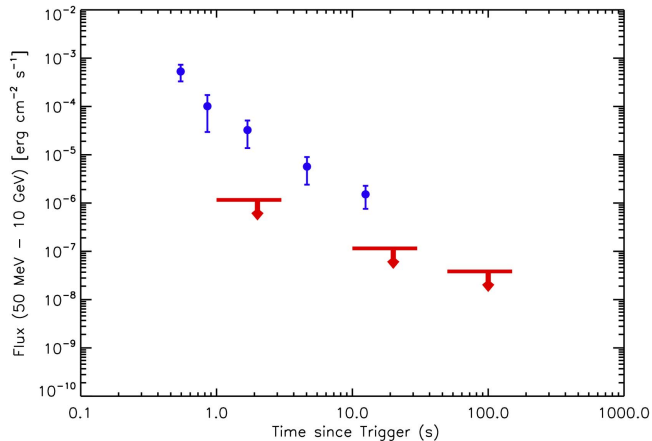


Figure 2. Gamma-ray light curve obtained by the AGILE-GRID for the short GRB 090510 repositioned at redshift $z = 0.18$ of GW170104 (blue points). The GRID upper limits obtained for the exposed fraction of the B arc of GW170104 at different timescales are marked in red.

acquisition for a 12.6 s segment starting at time $T_1 = 10:11:47.4$ UTC and ending at $T_2 = 10:12:00.0$ UTC. This event occurred on the 16 ms trigger timescale for which the average MCAL occurrence rate²⁰ is 7.5×10^{-3} Hz. Interestingly, this time interval includes the GW170104 detection time T_0 . Analysis in this time interval reveals a

²⁰ This rate is dominated by background events. An analysis of the triggered MCAL data with 16 ms bin shows that the rate of data acquisitions with peaks of signal-to-noise ratio (S/N) above 5σ is $\sim 5 \times 10^{-4}$ Hz.

significant peak at the onboard trigger time $T_{E1} = T_0 - 6.87$ s (10:11:51.70 \pm 0.05 s UTC, that we call “E1”). This event appears to be significant with 26 ms binning resulting in 37 raw counts in the full energy band and a preliminary signal-to-noise ratio (S/N) of 5.2σ . After having carried out standard off-line processing and event pile-up removal, the E1 S/N ratio becomes 3.6σ . Furthermore, two more events within 1 s from T_0 are noticed in the raw telemetry for the full MCAL energy band. An event (that we call “E2”) occurred at $T_{E2} = T_0 - 0.46$ s (10:11:58.10 \pm 0.05 s UTC) and is significant with 32 ms binning. This event shows 37 raw counts and a pre-filtering S/N ratio of 4.2σ . After filtering and pile-up removal its S/N ratio slightly increases to 4.4σ (see Figure 4). A third feature after T_0 (that we call “E3”) is noticed in the 96 ms binned light curve occurring on $T_{E3} = T_0 + 0.30$ s (10:11:58.90 \pm 0.05 s UTC). This feature shows 89 raw counts and a pre-filtering S/N ratio of 3.7σ . After filtering and pile-up removal its S/N ratio is 3σ (in Figure 5 a 4 s interval centered at E2 time of the 32 ms light curve, in the full band and in the $E \leq 1.4$ MeV, $E \geq 1.4$ MeV energy bands).

Therefore, with these preliminary indications, we focused on detecting signals in specific time bins that turned out to be the most effective ones in revealing short GRBs as detected by the AGILE-MCAL. We performed a refined search (with time shifts) in three binning timescales (26, 32, and 96 ms). One relevant timescale is of the order of 100 ms as demonstrated by the range of T_{50} measured in MCAL data (see Figure 4 of Galli et al. 2013). This timescale is optimal for searching emission during the prompt phase of short GRBs (e.g., GRB 090510,

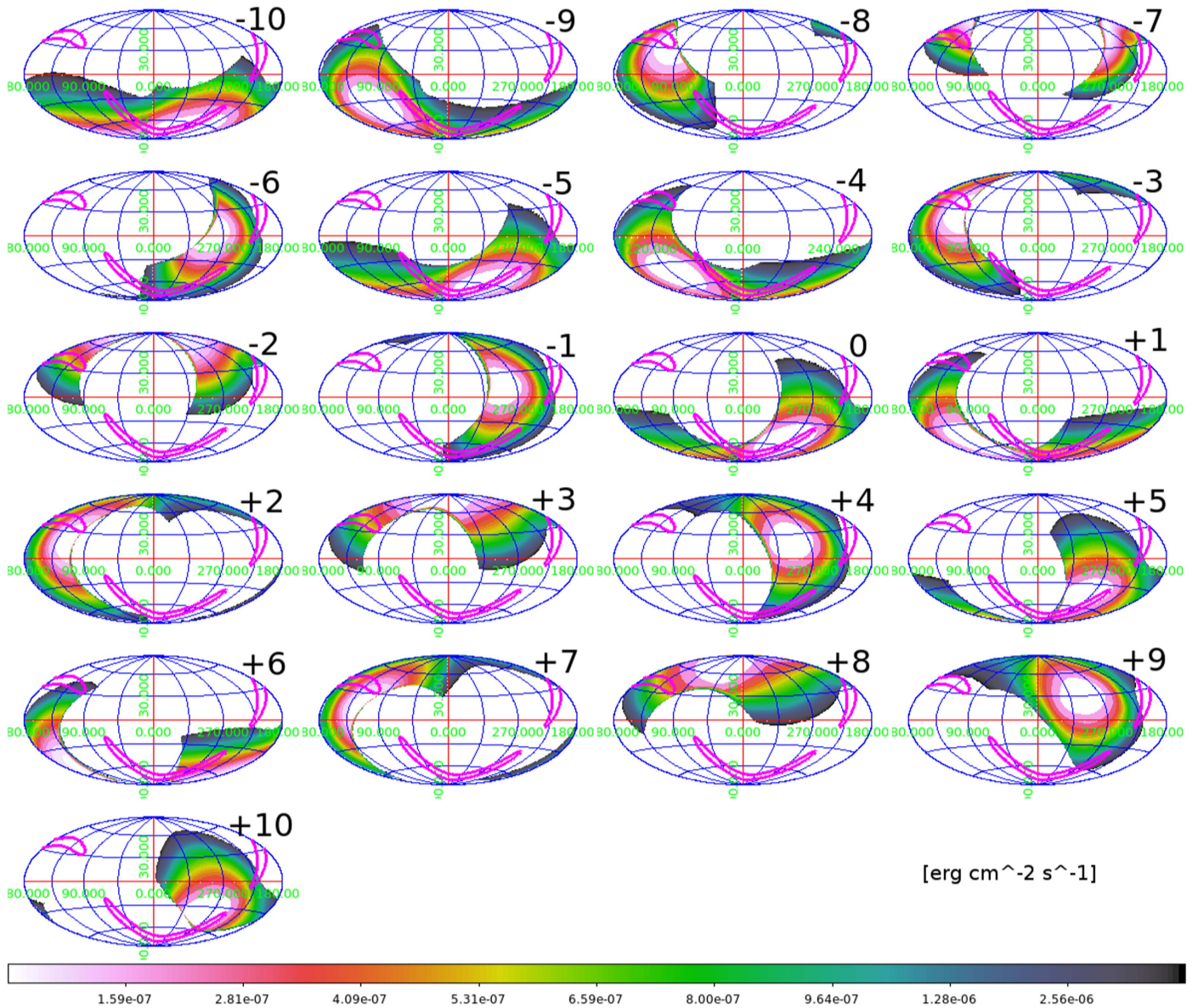


Figure 3. Sequence of ($E > 50$ MeV) maps in Galactic coordinates showing the AGILE-GRID passes with the best sensitivity (in $\text{erg cm}^{-2} \text{s}^{-1}$) over the GW170104 LR obtained during the period (-1000 s, $+1000$ s) with respect to T_0 . The color maps show the gamma-ray flux 3σ upper limits in the range 50 MeV–10 GeV with the most stringent values being $UL = (1-2) \times 10^{-8} \text{ erg cm}^{-2} \text{ s}^{-1}$. The sequence shows 21 maps for all the one-orbit passes of Table 1, corresponding to the 100 s interval numbers (from top left to bottom right): from -10 to $+10$. The GW170104 LR is marked by the purple contour, the LALInference 90% c.l. (The LIGO Scientific Collaboration & Virgo Collaboration 2017c).

and more recently GRB 170127C; Ursi et al. 2017). The other two timescales (26 and 32 ms) are chosen to optimize searches of “GRB 090510-precursor-like events” known to last between 20 and 30 ms. The latter class of events constitutes the physical reference of our optimized onboard trigger logic for data acquisition that AGILE implemented since November 2016 to improve its sensitivity to GW events. We applied to each binned light curve different phase shifts: 4 equally spaced shifts for the 32 and 96 ms binned light curves and 2 shifts for the 26 ms one, corresponding to shifts of 1/4 and 1/2 of the time bins, respectively. These events/features are presented in the 32 ms binned light curve of Figure 4 showing filtered and pile-up removed data. We verified that the South Atlantic Anomaly passage occurs ~ 1700 s after T_0 .

In order to assess the post-trial probability of detecting these three events close to T_0 we developed a targeted procedure to

identify untriggered peaks with the characteristics of E1, E2, and E3, within their respective light curves (of binning equal to 26, 32, and 96 ms). This procedure was carried out over a time interval of 2 weeks centered at T_0 , for a total livetime of 104,557 s. Given the MCAL filtered telemetry, this analysis produces FARs for these events and specific choices of time binning. The results²¹ are: $\text{FAR}_{E1} = 1 \times 10^{-3}$ Hz for 26 ms binning, $\text{FAR}_{E2} = 1 \times 10^{-4}$ Hz for 32 ms binning, and $\text{FAR}_{E3} = 3 \times 10^{-3}$ Hz for 96 ms binning. Only event E2 potentially emerges as an interesting candidate; further analysis supports this conclusion. It is then important to obtain the FARs for the 26 and 96 ms binned light curves corresponding to detections with the same S/N of E2. We obtained

²¹ Our signal is a superposition of Poisson noise and sparse non-Poissonian events. We conservatively ignore the subtraction of the latter events and determine the FAR as deduced from the total signal.

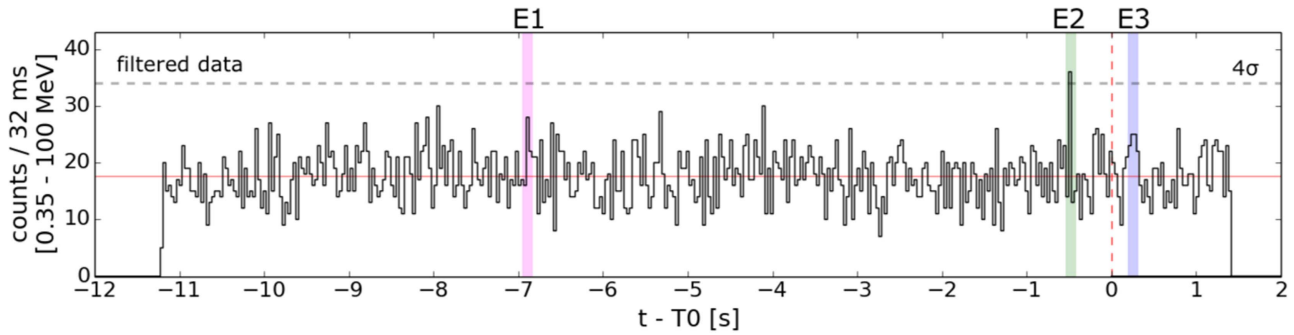


Figure 4. Light curve of MCAL data that includes the GW170104 event time. Data are displayed with a 32 ms time binning for the MCAL full energy band (0.35–100 MeV), after refined data processing. The E1, E2, and E3 event times are marked by vertical magenta, green, and light blue lines, while the T_0 is marked by a dashed red line. The horizontal dashed gray line indicates the 4σ level, estimated on the whole data acquisition interval (12.6 s). The orange horizontal line marks the average background level.

Table 1
Analysis of Individual Passes over the GW170104 Localization Region

Interval Number	Bin Central ^a Time	3σ UL ^b Range	Fraction ^c		
			Total	B	A
-10	-950	2.9/84.0	50%	100%	20%
-9	-850	4.1/105.0	72%	100%	10%
-8	-750	2.9/95.0	39%	22%	53%
-7	-650	11.0/59.0	34%	0%	62%
-6	-550	8.5/108.0	33%	62%	10%
-5	-450	2.9/74.0	50%	100%	9%
-4	-350	4.1/91.0	63%	100%	36%
-3	-250	2.9/103.0	36%	20%	58%
-2	-150	7.9/51.0	32%	0%	58%
-1	-50	11.0/89.0	30%	56%	9%
0	0	2.9/110.0	36%	64%	9%
+1	+50	4.5/98.0	43%	56%	33%
+2	+150	3.0/66.0	32%	0%	28%
+3	+250	5.9/42.0	32%	0%	29%
+4	+350	17.0/105.0	25%	19%	5%
+5	+450	3.0/42.0	25%	8%	5%
+6	+550	4.8/110.0	29%	17%	12%
+7	+650	3.2/73.0	30%	29%	1%
+8	+750	4.8/33.0	31%	29%	2%
+9	+850	34.0/108.0	15%	10%	5%
+10	+950	3.2/54.0	15%	10%	5%

Notes.

^a Centroid of the window time interval with respect to T_0 , $t - T_0$, in seconds.

All integrations have a duration of 100 s.

^b 3σ flux upper limit (10^{-8} erg cm^{-2} s^{-1}) obtained for emission in the range 50 MeV–10 GeV and for a spectrum assumed to be similar to the delayed gamma-ray emission of the short GRB 090510.

^c Fraction of the GRID exposed whole LVC LR of GW170104 and of the B and A arcs, respectively.

1.6×10^{-4} and 5.7×10^{-5} Hz for the 26 and 96 ms binned light curves, respectively. We take $\text{FAR}_{E2} = 1 \times 10^{-4}$ Hz as representative of our search of events similar to E2. In addition to the refined search binnings, for completeness in the analysis of the relevant timescales in the number of trials calculation, we also include the 16 and 64 ms unshifted binnings that refer to the onboard trigger logic timescales initially used for our data processing. We determine the FARs with the same S/N of E2 to be 2.4×10^{-4} and 7.5×10^{-5} Hz, respectively.

Having obtained the FAR over a 2-week timescale, we then estimate the post-trial probability P of these events accidentally

occurring within a time interval δt from T_0 with two different methods. The first one follows the formalism and definition laid out by Connaughton et al. (2016) for the analysis of *Fermi*-GBM data of GW150914. In that work, the probability is defined as $P = N \times \text{FAR} \times \delta t \times (1 + \ln(\Delta t/t_{\text{bin}}))$, where N is the number of trials, FAR is the false-alarm rate, δt is the time difference between the event time and T_0 , Δt is the one-sided time interval over which the search is done, and t_{bin} is the time binning used in the analysis. We considered as an event of interest only E2 for which we obtained: $P^{E2} = 12 \times (1 \times 10^{-4} \text{ Hz}) \times (0.46 \text{ s}) \times (2 + \ln(11.2 \text{ s}/0.016 \text{ s}) + \ln(1.4 \text{ s}/0.016 \text{ s})) \approx 0.00719$ ($\sim 2.4\sigma$), where we included both the backward and forward time intervals Δt of 11.2 and 1.4 s, respectively, and $\delta t = 0.46$ s. We adopted a factor of $N = (4 \times 2) + (2 \times 1) + 1 + 1 = 12$ to take into account the number of trials implemented in the refined analysis procedure, which includes three independent searches and their corresponding time shifts. This number of trials is over-estimated because the results for overlapping phase shifts are not independent and for the effect of unsubtracted non-Poissonian events in the FAR calculation.

The second method to estimate the post-trial probability of E2 is based on an independent procedure. We considered the whole MCAL data stream of the same two weeks used for FAR estimate with “a posteriori” choices: 32 ms binning and fixed time shift. We simulated the occurrence of an external trigger, at a random time t^* , and determined the time difference (τ) between t^* and the closest peak with $S/N \geq 4.4\sigma$. This procedure was repeated 6 million times and produced a distribution of τ . We determine the probability of occurrence of a signal with characteristics similar to E2 ($\tau \leq 0.46$ s) to be 3.7×10^{-3} that corresponds to 2.7σ . We consider this value to be an alternative estimate of the post-trial probability of E2 events.

We conclude that the E2 event turns out to have a post-trial coincidence probability between 2.4σ and 2.7σ .

5. Discussion

AGILE observed the field containing GW170104 with good coverage and significant gamma-ray exposure of its LR. The AGILE-GRID exposed 36% of the B arc at the detection time T_0 . No transient gamma-ray source was detected near T_0 over timescales of 2, 20, and 200 s starting at T_0 . Figure 2 shows these prompt upper limits compared to a rescaled gamma-ray light curve of GRB 090510. Our gamma-ray upper limits are quite relevant in constraining prompt gamma-ray emission

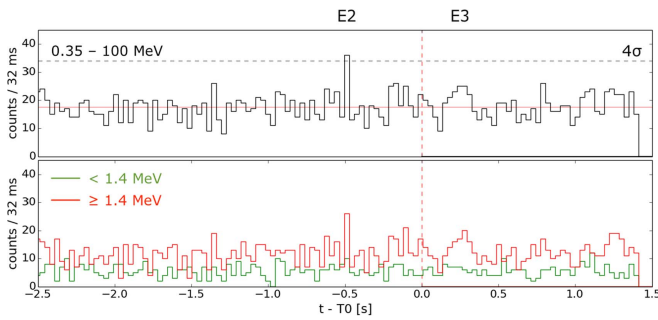


Figure 5. MCAL light curve binned at 32 ms for the 4 s time interval centered on the E2 event. Data displayed for the MCAL full energy band (0.35–100 MeV; top panel), and for the soft (≤ 1.4 MeV) and hard (≥ 1.4 MeV) energy bands (bottom panel). The GW170104 event time is at the origin of the abscissa. In the top panel, the horizontal dashed gray line indicates the 4σ level, estimated on the whole data acquisition interval (12.6 s). The orange horizontal line marks the average background level.

from GW170104. Furthermore, we obtain constraints for gamma-ray emission above 50 MeV also for possible precursor and delayed emission as detailed in Table 1. It is important to note that the co-axial SA detector had a partial coverage of the GW170104 LR at T_0 (within 1s) that was observed between 0° and 30° off-axis. No significant detection was obtained by SA imaging or ratemeter data in the 20–60 keV band during the time interval $T_0 \pm 100$ s for a stable background. The 3σ UL has been derived for a 1 s integration time and varies between $F^{\text{SAc}} = 1.5 \times 10^{-8}$ erg cm^{-2} for an on-axis position and $F^{\text{SAs}} = 6.6 \times 10^{-8}$ erg cm^{-2} at 30° off-axis position. A search in the SA ratemeter data does not produce a significant detection with a 2σ fluence upper limit of 2.4×10^{-8} erg cm^{-2} (1 s integration time).

MCAL detected three short-timescale events/features, of which only one remained significant after a refined analysis. The E2 event has a pre-trial S/N ratio of 4.4σ , and a post-trial probability of occurring within 0.46 s before T_0 between 2.4σ and 2.7σ . This event is the most interesting and is worthy of additional investigation and searches for possible coincident detections by other space instruments. We estimated the observed energy flux in the energy range 0.4–40 MeV at two positions on the B arc and at one on the A1 arc. We used a mean photon index taking into account the detector response and fitted the normalization parameter. We obtained on the B arc $F_{Bc} = 2.8_{-1.0}^{+1.9} \times 10^{-6}$ erg $\text{cm}^{-2} \text{s}^{-1}$, assuming a power-law model with a fixed mean photon index of -2 and estimating it at the a position with the best sensitivity (on-axis), while $F_{Bs} = 2.5_{-1.0}^{+2.7} \times 10^{-6}$ erg $\text{cm}^{-2} \text{s}^{-1}$ with the same photon index at a position with lower sensitivity. For the A1 arc, we obtained $F_{A1} = 3.7_{-1.4}^{+5.1} \times 10^{-6}$ erg $\text{cm}^{-2} \text{s}^{-1}$ with the same photon index. We consider the F_{Bc} value the best flux estimate for the B arc, corresponding to a fluence $F'_{Bc} = 8.9_{-3.0}^{+6.1} \times 10^{-8}$ erg cm^{-2} . Moreover, we evaluate the flux at this position also assuming a photon index of -1.6 (observed, e.g., during the prompt phase of GRB 090510), obtaining $F_{hBc} = 4.6_{-2.0}^{+5.5} \times 10^{-6}$ erg $\text{cm}^{-2} \text{s}^{-1}$ and $F'_{hBc} = 1.5_{-0.6}^{+1.8} \times 10^{-7}$ erg cm^{-2} .

We obtained the fluence extrapolations to the SA energy band to be $\sim 2.1 \times 10^{-8}$ erg cm^{-2} for photon index of -2 and $\sim 4.8 \times 10^{-9}$ erg cm^{-2} for -1.6 . We note that the SA UL fluence at the center of its FoV, F^{SAc} , is slightly lower than the former value, therefore providing a constraint on the spectrum. The latter value of the extrapolated fluence for the

index of -1.6 is not constrained by the SA observations. We also checked the extrapolation of the E2 flux to the GRID energy band and compared it to the 2 s UL fluence. We obtained an extrapolated fluence at energies above 50 MeV of $\sim 8.9 \times 10^{-8}$ erg cm^{-2} for a -2 photon index. Again, we end up with a lower value with respect to the GRID 2 s UL fluence, 5.8×10^{-6} erg cm^{-2} .

In conclusion, for the GW170104's most likely distance of 880 Mpc (Abbott et al. 2017), we obtain for the E2 event in the MCAL band an isotropic luminosity $L_{\text{iso}} = 2.6 \times 10^{50}$ erg s^{-1} and total energy $E_{\text{iso}} = 8.3 \times 10^{48}$ erg.

It is interesting to note that the E2 event appears to be quite similar in its timing and flux characteristics compared to the precursor event detected about 0.46 s before the onset of the brightest part of the short GRB 090510. This weak precursor was simultaneously detected by the AGILE-MCAL and *Fermi*-GBM (Abdo et al. 2009; Giuliani et al. 2010) and was therefore confirmed by the simultaneous detection of two space instruments. In our case, this precursor of GRB 090510 played an important role in calibrating the new MCAL data acquisition system that has been optimized just for GW counterpart searches. We notice that both the triggering events E1 and E2 (which occurred within the telemetered time window after E1) satisfy flux and timing conditions set up following the MCAL detection of the GRB 090510 precursor²². The E2 event appears to be harder than the 2009 precursor.

If associated with GW170104, the E2 event shows interesting physical properties. Its fluence and L_{iso} are comparable to those of weak short GRBs previously detected by several space instruments. A total energy estimated in the isotropic approximation of $\sim 10^{49}$ erg is 10^{-7} times smaller than the total black hole rest mass of $50 M_\odot c^2$. Beaming effects would make this ratio even smaller. It is clear that if any association between E2 and GW170104 were confirmed by simultaneous detections of different instruments, the e.m. output following the GW170104 gravitational coalescence would be severely constrained. MCAL cannot determine the position of the event in the absence of simultaneous onboard detection by the GRID or SA. However, from Figure 1 we obtain the definite sky region belonging to the B arc that was not occulted by the Earth and exposed by MCAL for off-axis angles up to 45° at the T_0 of GW170104. We also have large off-axis angle MCAL exposures for regions labeled A1 and A2 in Figure 1.

6. Conclusions

The LVC detection of GW170104 produced by a BH–BH coalescence of a total mass of $50 M_\odot$ is a remarkable event, the third in the LVC series of confirmed detections. AGILE data are useful in assessing the possible e.m. emission associated with GW events. AGILE already obtained interesting upper limits for gamma-ray and hard X-ray emission from the first GW event, GW150914 (Tavani et al. 2016). In that case, the AGILE-GRID exposure of the LVC LR occurred 100 s before and 300 s after the event T_0 .

GW170104 is much more interesting from the point of view of AGILE observations. In this case, significant exposure of the LR was obtained simultaneously with the detection time T_0 .

²² The MCAL triggering procedure allows only one trigger within the allocated time window following a first event. The E2 event could have independently triggered the MCAL system, but it did not because it was too close to E1.






The gamma-ray and hard X-ray upper limits obtained by the GRID and SA are therefore even more constraining than for GW150914.

Even more interestingly, we identify in the MCAL data the E2 candidate event with noticeable characteristics. We note its similarity in flux and timing properties to the precursor of the short GRB 090510. Our estimate of the post-trial probability of being temporally associated with GW170104 (2.4σ – 2.7σ). As in the case of the GBR 090510 precursor, a confirmation by different space instruments would provide the definite proof of its association with the GW.

AGILE continues its observations of the sky in spinning mode and is fully operational in the search of GW source counterparts.

We thank the LIGO/Virgo Collaboration for sharing information on GW170104 and for discussion and comments on our manuscript. In particular, we thank F. Ricci, M. Branchesi, L. Singer, and E. Katsavounidis. We thank the anonymous referee for the comments. We thank the ASI management, the technical staff at the ASI Malindi ground station, the technical support team at the ASI Space Science Data Center, and the Fucino AGILE Mission Operation Center. AGILE is an ASI space mission developed with programmatic support by INAF and INFN. We acknowledge partial support through ASI grant No. I/028/12/2.

ORCID iDs

M. Tavani  <https://orcid.org/0000-0003-2893-1459>
 P. Munar-Adrover  <https://orcid.org/0000-0002-1942-7376>
 G. Piano  <https://orcid.org/0000-0002-9332-5319>
 A. Morselli  <https://orcid.org/0000-0002-7704-9553>
 S. Vercellone  <https://orcid.org/0000-0003-1163-1396>

References

- Abbott, B. P., Abbott, R., Abbott, T. D., et al. 2016a, *PhRvD*, **93**, 122003
 Abbott, B. P., Abbott, R., Abbott, T. D., et al. 2016b, *PhRvL*, **116**, 131103
 Abbott, B. P., Abbott, R., Abbott, T. D., et al. 2016c, *PhRvL*, **116**, 241103
 Abbott, B. P., Abbott, R., Abbott, T. D., et al. 2016d, *PhRvL*, **116**, 061102
 Abbott, B. P., Abbott, R., Abbott, T. D., et al. 2016e, *PhRvD*, **93**, 122004
 Abbott, B. P., Abbott, R., Abbott, T. D., et al. 2016f, *PhRvL*, **116**, 241102
 Abbott, B. P., Abbott, R., Abbott, T. D., et al. 2017, *PhRvL*, **118**, 221101
 Abdo, A. A., Ackermann, M., Ajello, M., et al. 2009, *Natur*, **462**, 331
 Ackermann, M., Ajello, M., Albert, A., et al. 2016, *ApJL*, **823**, L2
 Bulgarelli, A., Trifoglio, M., Gianotti, F., et al. 2014, *ApJ*, **781**, 19
 Connaughton, V., Burns, E., Goldstein, A., et al. 2016, *ApJL*, **826**, L6
 Del Monte, E., Barbiellini, G., Donnarumma, I., et al. 2011, *A&A*, **535**, A120
 Fuschino, F., Labanti, C., Galli, M., et al. 2008, *NIMPA*, **588**, 17
 Galli, M., Marisaldi, M., Fuschino, F., et al. 2013, *A&A*, **553**, A33
 Giuliani, A., Fuschino, F., Vianello, G., et al. 2010, *ApJL*, **708**, L84
 Giuliani, A., Longo, F., Verrecchia, F., et al. 2013, *GCN*, **15479**, 1
 Giuliani, A., Mereghetti, S., Fornari, F., et al. 2008, *A&A*, **491**, L25
 Giuliani, A., Mereghetti, S., Marisaldi, M., et al. 2014, *A&A*, submitted (arXiv:1407.0238)
 Labanti, C., Marisaldi, M., Fuschino, F., et al. 2009, *NIMPA*, **598**, 470
 Longo, F., Giuliani, A., Marisaldi, M., et al. 2013, *GCN*, **14344**, 1
 Longo, F., Moretti, E., Nava, L., et al. 2012, *A&A*, **547**, A95
 Marisaldi, M., Fuschino, F., Tavani, M., et al. 2014, *JGRA*, **119**, 1337
 Marisaldi, M., Labanti, C., Fuschino, F., et al. 2008, *A&A*, **490**, 1151
 Moretti, E., Longo, F., Barbiellini, G., et al. 2009, *GCN*, **9069**, 1
 Pittori, C. 2013, *NuPhS*, **239**, 104
 Singer, L. P., & Price, L. R. 2016, *PhRvD*, **93**, 024013
 Tavani, M., Barbiellini, G., Argan, A., et al. 2009, *A&A*, **502**, 995
 Tavani, M., Marisaldi, M., Labanti, C., et al. 2011, *PhRvL*, **106**, 018501
 Tavani, M., Pittori, C., Verrecchia, F., et al. 2016, *ApJL*, **825**, L4
 Tavani, M., Ursi, A., Fuschino, F., et al. 2017a, *GCN*, **20375**, 1
 Tavani, M., Verrecchia, F., Minervini, G., et al. 2017b, *GCN*, **20395**, 1
 The LIGO Scientific Collaboration & Virgo Collaboration 2017a, *GCN*, **20364**, 1
 The LIGO Scientific Collaboration & Virgo Collaboration 2017b, *GCN*, **21056**, 1
 The LIGO Scientific Collaboration & Virgo Collaboration 2017c, *GCN*, **20385**, 1
 Ursi, A., Munar-Adrover, P., Verrecchia, F., et al. 2017, *GCN*, **20545**, 1
 Veitch, J., Raymond, V., Farr, B., et al. 2015, *PhRvD*, **91**, 042003
 Verrecchia, F., Pittori, C., Giuliani, A., et al. 2013, *GCN*, **14515**, 1